




CDK4/6 inhibitors induce breast cancer senescence with enhanced anti-tumor immunogenic properties compared with DNA-damaging agents

Dong Hyun Lee^{1,2,3} , Muhammad Imran^{1,3}, Jae Ho Choi^{3,4}, Yoo Jung Park⁴, Young Hwa Kim³, Sunwoo Min⁵, Tae Jun Park^{1,2,3}  and Yong Won Choi^{3,4} 

1 Department of Biochemistry and Molecular Biology, Ajou University School of Medicine, Suwon, Korea

2 Department of Biomedical Sciences, Ajou University Graduate School of Medicine, Suwon, Korea

3 Inflamm-Aging Translational Research Center, Ajou University Medical Center, Suwon, Korea

4 Department of Hematology-Oncology, Ajou University School of Medicine, Suwon, Korea

5 Department of Biological Sciences, Korea Advanced Institute of Science and Technology (KAIST), Daejeon, Korea

Keywords

CDK4/6 inhibitors; DNA-damaging agents; SASP; therapy-induced senescence; tumor microenvironment

Correspondence

T. J. Park, Department of Biochemistry and Molecular Biology, Ajou University School of Medicine, 164 Worldcup-ro, Yeongtong-gu, Suwon 16499, Korea
Fax: 82 31 219 5059
Tel: 82 31 219 5055
E-mail: park64@ajou.ac.kr

Y. W. Choi, Department of Hematology-Oncology, Ajou University School of Medicine, 164 Worldcup-ro, Yeongtong-gu, Suwon 16499, Korea
Fax: 82 31 219 5983
Tel: 82 31 219 5141
E-mail: dreamliebe@ajou.ac.kr

Dong Hyun Lee and Muhammad Imran contributed equally to this work

Abbreviations

AI, aromatase inhibitors; APCs, antigen-presenting cells; BP, biological process; CC, cellular component; CDK, cyclin-dependent kinase; CDK4/6i, cyclin-dependent kinase inhibitors; Cis, cisplatin; DDR, DNA damage and repair; DEGs, differentially expressed genes; Doxo, doxorubicin; ELISA, enzyme-linked immunosorbent assay; ET, endocrine therapy; GO, Gene ontology; GOBP, Gene ontology biological process; GOMF, Gene ontology molecular function; GSEA, Gene set enrichment analysis; IFN, interferons; IPA, ingenuity pathway analysis; ISG, interferon-stimulated genes; Max, maximum; MDSC, myeloid-derived suppressor cell; MEF, mouse embryonic fibroblast; MHC, major histocompatibility complex; Min, minimum; MMC, mitomycin; NES, normalized enrichment score; NF- κ B, nuclear factor-kappa-B; NK cells, natural killer cells; NKG2D, natural killer cells group 2 member D; Palbo, Palbociclib; PCR, polymerase chain reaction; PDAC, pancreatic ductal adenocarcinoma; PIDD, p53-inducible death-domain containing protein; RB, retinoblastoma protein; SAHF, senescence-associated heterochromatin foci; SASP, senescence-associated secretory phenotypes; SA- β -gal, senescence-associated beta galactosidase; TGF- β , transforming growth factor-beta; TIS, therapy-induced senescence; TME, tumor microenvironment; TNBC, triple-negative breast cancer; TNF α , tumor necrosis factor-alpha.

Since therapy-induced senescence (TIS) can either support or inhibit cancer progression, identifying which types of chemotherapeutic agents can produce the strongest anti-tumor TIS is an important issue. Here, cyclin-dependent kinase4/6 inhibitors (CDK4/6i)-induced senescence was compared to the TIS induced by conventional DNA-damaging agents. Despite both types of agents eliciting a similar degree of senescence, we observed increased expression of the senescence-associated secretory phenotype (SASP) and ligands related to pro-tumor immunity (*IL6*, *CXCL8*, *TGF β* , *CD274*, and *CEACAM1*) and angiogenesis (*VEGFA*) mainly in TIS induced by DNA-damaging agents rather than by CDK4/6i. Additionally, although all agents increased the expression of anti-tumor immunomodulatory proteins related to antigen presentation (*MHC-I*, *B2M*) and T cell chemokines (*CXCL9*, *10*, *11*), CDK4/6i-induced senescent cells still maintained this expression at a similar or even higher intensity than cells treated with DNA-damaging agents, despite the absence of nuclear factor-kappa-B (NF- κ B) and p53 activation. These data suggest that in contrast with DNA-damaging agents, which augment the pro-tumorigenic microenvironment via pro-inflammatory SASP, CDK4/6i can generate TIS only with antitumor immunomodulatory proteins.

(Received 22 May 2023, revised 5 October 2023, accepted 17 October 2023, available online 2 November 2023)

doi:10.1002/1878-0261.13541

1. Introduction

Therapy-induced senescence (TIS), elicited by various chemotherapeutic agents and radiotherapy, has been regarded as one of the essential tumor suppressive mechanisms of current therapeutics [1–3]. However, the accumulation of senescent cells both in tumor and normal tissues can be detrimental by promoting tumor relapse, metastasis, and resistance to therapy by facilitating proliferation [4], angiogenesis [5], epithelial–mesenchymal transition [6], cell survival [7], and immune escape [8]. Moreover, senescent cells in normal tissue can contribute to therapy-induced adverse effects [9]. The potential detrimental effects of TIS are mediated by the release of senescence-associated inflammatory phenotype (SASP) that can modulate the tumor microenvironment (TME). Pro-inflammatory SASP (IL-1, IL-6, CXCL8, TNF α) [10] and expression of pro-angiogenic factors (VEGFA, GDF15) [11,12] suppress anti-tumor immunity, whereas some types of SASP can activate anti-tumor immunity by augmenting tumor antigen presentation (Interferon family; IFN), cytotoxic T cell infiltration (CXCL9, CXCL10, CXCL11) [13], and activation of NK cells and T cells (IL-2, MICB) [14,15]. Moreover, senescent cells present in the TME can either facilitate or impede angiogenesis by releasing pro-angiogenic (VEGFA) or anti-angiogenic (MMRN2) factors [12,16,17], respectively. Therefore, it is of utmost importance to maximize the secretion of SASP linked to anti-tumor immunity and to minimize those that instigate pro-tumor immunity responses. Hence, by better understanding the mechanisms that regulate pro- and anti-tumor SASP independently, it may be possible to develop more effective senescence inducers that preserve the ability to arrest the cell cycle and release SASP associated with the anti-tumor activity.

Since a prior study demonstrated that fibroblasts overexpressing p16^{INK4A} exhibit all the features of senescence but lack SASP [18], CDK4/6 inhibitors (CDK4/6i), as a mimic of p16^{INK4A} activation, can be a proper candidate of an ideal senescence inducer. However, unlike senescent fibroblasts overexpressing p16^{INK4A}, CDK4/6i-induced senescent cells excrete a range of SASP factors [19,20]. Nevertheless, recent studies reveal that CDK4/6i treatment can elicit anti-tumor immunity by targeting tumor

cells and regulatory T cells and can also synergize with immune checkpoint inhibitors [21–23]. It is, therefore, still interesting to investigate whether senescent cancer cells induced by CDK4/6i treatment have a stronger ability to create the anti-tumor immune microenvironment compared to other conventional chemotherapeutic DNA-damaging agents. However, to the best of our knowledge, no systematic comparative study of the characteristics of DNA-damaging agent-induced and CDK4/6i-induced senescent cancer cells, particularly in terms of the expression patterns of SASP and ligands that modulate the TME, has been conducted. Therefore, we examined the effects of representative DNA-damaging agents (Cisplatin, Doxorubicin, Etoposide, and Carboplatin) and a CDK4/6i (Palbociclib, Abemaciclib) on the senescence of CDK4/6i-sensitive breast cancer cells. We found that CDK4/6i-induced senescent cancer cells induced strong expression of SASP and ligands related to an anti-tumor immunity, which was comparable with that induced by DNA-damaging agent-induced senescence. Furthermore, CDK4/6i led to significantly lower expression of SASP and ligands related to angiogenesis and pro-tumor immunity modulation.

2. Materials and methods

2.1. Cell culture and reagents

The breast cancer MCF-7 (RRID: CVCL_0031, KCLB No. 30022, Korean Cell Line Bank, Seoul, Korea) and HCC1428 (RRID: CVCL_1253, KCLB No. 9S1428, Korean Cell Line Bank, Seoul, Korea) cells were cultured (1×10^5 cells/60 mm culture dish) in RPMI 1640 (WELGENE, Gyeongsan, Korea) supplemented with 10% heat-inactivated fetal bovine serum (FBS, GIBCO-BRL, Grand Island, NY), 1% penicillin and streptomycin and maintained at 37 °C under 5% CO₂ in a humidified atmosphere. The cell lines used in this study were authenticated by short-tandem-repeat profiling and were tested negative for mycoplasma contamination (e-MycoTM plus Mycoplasma PCR Detection Kit, Cat. No 25237, Seongnam, Korea). DNA-damaging agents including Doxorubicin, Cisplatin, Etoposide, and Carboplatin, CDK4/6i including Palbociclib, Abemaciclib, and Ribociclib, and aromatase inhibitors (AI) including

Anastrozole, Letrozole (Selleck, Houston, TX) were treated to the cells. Antibodies purchased from Cell Signaling Technology (CST, Danvers, MA) include pRb (#9308), pAKT (#3787S), AKT (#9272), pErk1/2 (#9106S), Erk1/2 (#9107S), p-p65 (#3031S), c-Jun (#9165), p-c-Jun (#2361S), and p-STAT3 (#4113S), Santa Cruz Biotechnology (SC, Dallas, TX); Rb (SC-50), STAT3 (SC-482), p53 (SC-126), p21^{Waf1/Cip1} (SC-6246), I κ B α (SC-1643), α -Tubulin (SC-32293), and β -Actin (SC-4778), Merck Millipore (Burlington, MA); anti- γ H2AX (05–636), Abcam (Cambridge, UK); anti-Lamin B1 (ab16048).

2.2. Induction of cancer cell senescence

For the induction of senescence, MCF-7 and HCC1428 cells were cultured and treated with DNA-damaging agents (Cisplatin, Doxorubicin, Etoposide, and Carboplatin) and CDK4/6i (Palbociclib, Abemaciclib, and Ribociclib) for 2 days. The media were changed after every 2 days and cells were harvested following 5 days of exposure to DNA-damaging agents and CDK4/6i.

2.3. Cell viability assay

MCF-7 cells were exposed to various concentrations of Anastrozole and Letrozole (2.5, 5, 10, 20, and 30 μ M). After 5 days of incubation with AI, cell viability assay was conducted using Cell Counting Kit-8 (D-PlusTM CCK cell viability assay kit, Cat. No. CCK-3000, Donginbiotech Co., Ltd, Seoul, Korea) according to the manufacturer's instructions. Briefly, cells were treated with WST in fresh cultured medium and incubated for 1 h at 37 °C under 5% CO₂ in a humidified atmosphere. Optical density was measured at 450 nm using an EonTM microplate spectrophotometer (BioTEK, Winooski, VT). Cell viability was calculated in comparison with control MCF-7.

2.4. SA- β -galactosidase staining

For SA- β -galactosidase staining, the control and drug-treated MCF-7 cells were washed twice with PBS, and then fixed with 4% paraformaldehyde for 5 min at room temperature in the dark. Cells were then washed three times with PBS and incubated with SA- β -gal staining solution (40 mM, pH 6 citrate/phosphate buffer, 5 mM each Ferro- and Ferricyanide, 150 mM NaCl, 2 mM MgCl₂ and 1 mg·mL⁻¹ X-gal) for 15 h at 37 °C in the dark. After the incubation, cells were washed again with PBS and observed under a bright field microscope (OLYMPUS IX71, Tokyo, Japan).

2.5. Cell cycle analysis

The control and drug-treated cells were harvested after 5 days of treatment, washed with PBS, and fixed in ice-cold 70% (vol/vol) ethanol. Cells were treated with RNAase A and stained with propidium iodide. The distribution of the cell cycle was then analyzed using flow cytometry (BD FACSAriaTM III, Franklin Lakes, NJ).

2.6. RNA extraction and qPCR

Total RNA was extracted from control and senescent MCF-7 cells using the QIAGEN (Hilden, Germany) RNA extraction kit and reverse transcribed using a cDNA synthesis kit (Invitrogen, Waltham, MA). qPCR was performed using iQ SYBR[®] Green Supermix qPCR Kit (Bio-Rad, Hercules, CA) on a CFX96TM Real-Time System (Bio-Rad, Hercules). Data were analyzed using the 2^(- $\Delta\Delta$ CT) method. β -actin was used as a control to normalize the expression of target genes. The primer sequences are given in Table S1.

2.7. Immunoblotting

The control and drug-treated MCF-7 cells were harvested after 5 days of treatment and lysed with RIPA buffer (50 mM Tris-HCl pH 7.5, 150 mM sodium chloride, 1 mM EDTA, 1% Nonidet P-40, 1% sodium deoxycholic acid, 0.1% SDS along with protease and phosphatase inhibitors). Proteins were quantified and subjected to SDS/PAGE. Immunoblotting was performed on nitrocellulose membrane and proteins were detected using the immunoblotting detection kit WESTA SAVE^{UP}TM (Seoul, Republic of Korea). The phosphorylated form and the total form of proteins on the same membrane were detected by stripping and reprobing the membrane. β -actin and α -tubulin were used as a loading control.

2.8. Enzyme-linked immunosorbent assay (ELISA)

MCF-7 cells (4 \times 10⁵ cells/100 mm dish) were cultured and treated with DNA-damaging agents and CDK4/6i for senescence induction, and the media were harvested after 5 days. Subsequently, the conditioned media were centrifuged and filtered through a 0.2- μ m pore size syringe filter. The secretions of VEGF, IL-6, and CXCL8 were assessed in the conditioned media using a human DuoSet ELISA kit (R&D Systems, Minneapolis, MN) according to the manufacturer's instructions. The levels of VEGF,

IL-6, and CXCL8 in the conditioned media were quantified using Eon™ microplate spectrophotometer (BioTEK, Winooski, VT).

2.9. RNA sequencing and transcriptome analysis

RNA was isolated from control and senescent MCF-7 cells using a QIAGEN extraction kit. RNA sequencing was carried out by Life & Science (LAS, Gimpo, South Korea). There were 60 million read-pairs per sample, and gene mapping was performed using the ALTAANALYZE (version 2.0) alignment tool. Extracted FASTQ files were aligned with reference genome version hg38. The total RNA transcriptomes of 15 290 genes were normalized by the “EdgeR” package (version 3.40.2) in R studio. Before transcriptome analysis, read counts of 0 or < 10 in all 12 samples were considered pseudogenes and were filtered out. Trimmed mean of M values (TMM) was used as normalized values to analyze differentially expressed genes (DEGs).

2.10. Data processing and visualization

To illustrate gene expression patterns, we calculated *z*-scores for 8832 DEGs. Sample correlations were evaluated using Spearman’s rank correlation coefficient. To compare gene expression profiles across all samples, we visualized a similarity index heatmap based on *z*-scores. These values were then input into Spearman’s rank correlation analysis. For normalized enrichment score (NES) analysis, we utilized the R package “Fgsea” with 1000 permutations. Reference gene sets for various gene set enrichment analysis (GSEA) categories were obtained from Msigdb in R. GSEA was performed both using the desktop application (GSEA 4.2.3) and TMM normalized values calculated through the “EdgeR” package. The following settings were used: collapse/Remap to gene symbols: collapse; permutation type: phenotype; chip platform: Human Ensemble Transcript ID MSigDB.vs.2023.1.Hs.Chip; enrichment statistic: weighted; metric for ranking genes: Signal2-Noise; gene list sorting mode: real; gene list ordering mode: descending; maximum size of gene sets, 500; and minimum size of gene sets: 15. To compare overlapping signature gene sets between the control and drug-induced senescence groups, cnetplots were generated using the “enrichplot” package and the “clusterprofiler” package. Ingenuity pathway analysis (IPA) was performed using QIAGEN IPA (version 42012434, Ingenuity Systems; Qiagen China Co., Ltd.) to identify pathways, top regulator effect networks, and gene signatures based on TMM values for drug-treated MCF-7

cells. All IPA analyses were conducted using a cutoff of $P \leq 0.05$ and log 2-fold change of ≥ 0.5 .

2.11. Statistical analysis

All experiments were repeated at least three times and the data were presented as mean + SD. Statistical significance was calculated using one-way ANOVA. $P \leq 0.05$ was regarded as statistically significant. The Spearman and Pearson correlation coefficients were applied to assess the correlation between samples.

3. Results

3.1. A similar extent of breast cancer cell senescence is induced by DNA-damaging agents and CDK4/6i

To characterize and compare senescence induced by treatment with DNA-damaging agents (Cisplatin and Doxorubicin) and CDK4/6i, we screened various breast cancer cell lines to find out which could achieve stable senescent status for analysis post-drug treatment. We selected MCF-7 (hormone receptor (HR): positive/human epidermal growth factor receptor 2 (HER2): negative) breast cancer cells harboring wild-type TP53 as a suitable model for studying the characteristics of TIS induced by different agents. In addition, since CDK4/6i are typically prescribed in conjunction with non-steroidal AI for the treatment of HR-positive and HER2-negative breast cancer patients, we conducted an analysis to determine whether AI could influence the process of CDK4/6i-induced senescence. Single treatments with AI at concentrations up to 30 μM demonstrated a slight but biologically insignificant compromise of cell viability (Fig. S1A), and combined treatment with AI and CDK4/6i revealed no additional effects on CDK4/6i-induced senescence (Fig. S1B). Therefore, CDK4/6i were applied alone in subsequent experiments. Since various types of agents, and even various concentrations of the same agent, can induce a significantly different senescent status in the same cancer cell line, it is important to identify the optimal concentrations and treatment conditions for each drug to induce similar levels of TIS. After treatment with the indicated concentrations of drugs for the indicated times, we detected comparable levels of SA- β -gal activity induced by DNA-damaging agents and CDK4/6i (Fig. 1A); however, the stage of cell cycle arrest was different; G2/M phase for DNA-damaging agents and G0/G1 phase for CDK4/6i (Fig. 1B). All therapeutic

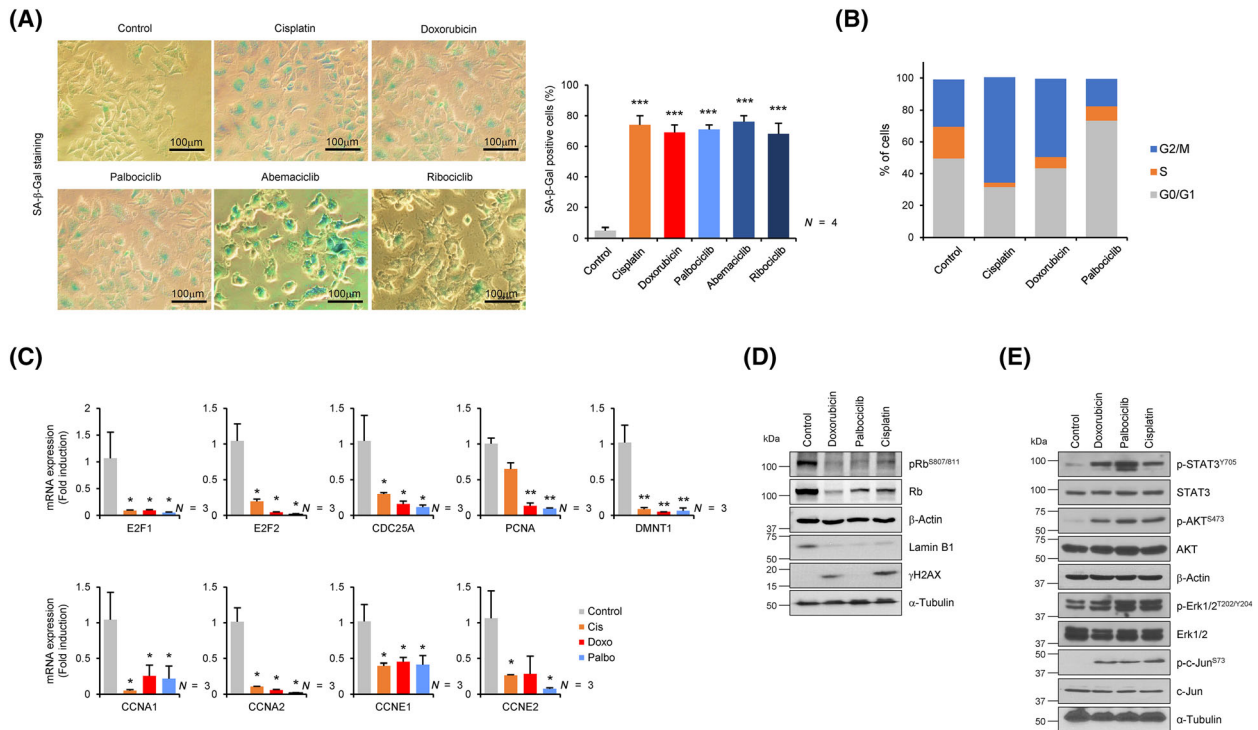


Fig. 1. A similar extent of senescence induction by DNA-damaging agents and CDK4/6i. (A) MCF-7 cells were treated with DNA-damaging agents (Cisplatin 5 μM and Doxorubicin 100 nM) and CDK4/6i (Palbociclib 2 μM, Abemaciclib 1 μM, and Ribociclib 5 μM) for 5 days and then SA-β gal staining was performed. Representative images of SA-β gal-positive cells are shown. Scale bar, 100 μm. The percentage of stained cells was quantified and presented as a bar graph. Data are mean ± SD of four ($N = 4$) independent experiments. The P -value was calculated using one-way ANOVA. *** $P < 0.001$. (B) Cell cycle analysis of control, DNA-damaging agents, and CDK4/6i-treated senescent cells was performed by FACS. A representative bar graph shows the percentage of cells in each cell cycle phase. (C) The mRNA expression of genes was measured using RT-qPCR in control, DNA-damaging agents, and CDK4/6i-induced senescent cells. The P -value was calculated by the one-way ANOVA. Data are mean ± SD of three ($N = 3$) independent experiments. * $P < 0.05$ and *** $P < 0.01$. (D, E) The cells were harvested after 5 days of drug treatment and subjected to immunoblotting for protein expression analysis. β-actin and α-tubulin were used as loading controls. Data are representative of three ($N = 3$) independent experiments.

agents reduced the expression of the E2F family and their well-known target genes to a similar extent (Fig. 1C), along with phosphorylated retinoblastoma (RB) (Fig. 1D). In addition, reduced expression of Lamin B1, widely recognized as a biomarker of senescence, was observed to a similar degree after treatment with different agents, while increased phosphorylation of γH2AX was observed only in senescent cells induced by DNA-damaging agents. This suggests that a meaningful DNA damage response was not activated in CDK4/6i-induced senescent cancer cells (Fig. 1D). In addition, to investigate the possibility that DNA-damaging agent- and CDK4/6i-induced senescence activate distinct pathways, we analyzed other important signaling pathways activation. Regardless of TIS type, increased phosphorylation of JNK, Erk1/2, STAT3, and AKT suggested that the JNK, MAPK, JAK/STAT, and AKT pathways were commonly activated by TIS, although phosphorylation of STAT3 in

CDK4/6i-induced senescent cells was slightly stronger than in DNA-damaging agent-induced senescent cells (Fig. 1E). Overall, our data suggest that DNA-damaging agents and CDK4/6i induce senescence in breast cancer cells to a similar extent.

3.2. Genes related to pro-inflammatory response, anti-tumor immunity, and angiogenesis are regulated differently in TIS by DNA-damaging agents and CDK4/6i

To clarify even slight differences in the expression of genes involved in not only SASP but also modulation of the TME, we examined changes in the whole transcriptome after TIS by using an RNA-sequence alignment tool. The expression pattern of 8832 genes arranged by hierarchical clustering was displayed as a heatmap. Comparison of TIS samples with parental control cells revealed definitive changes in the

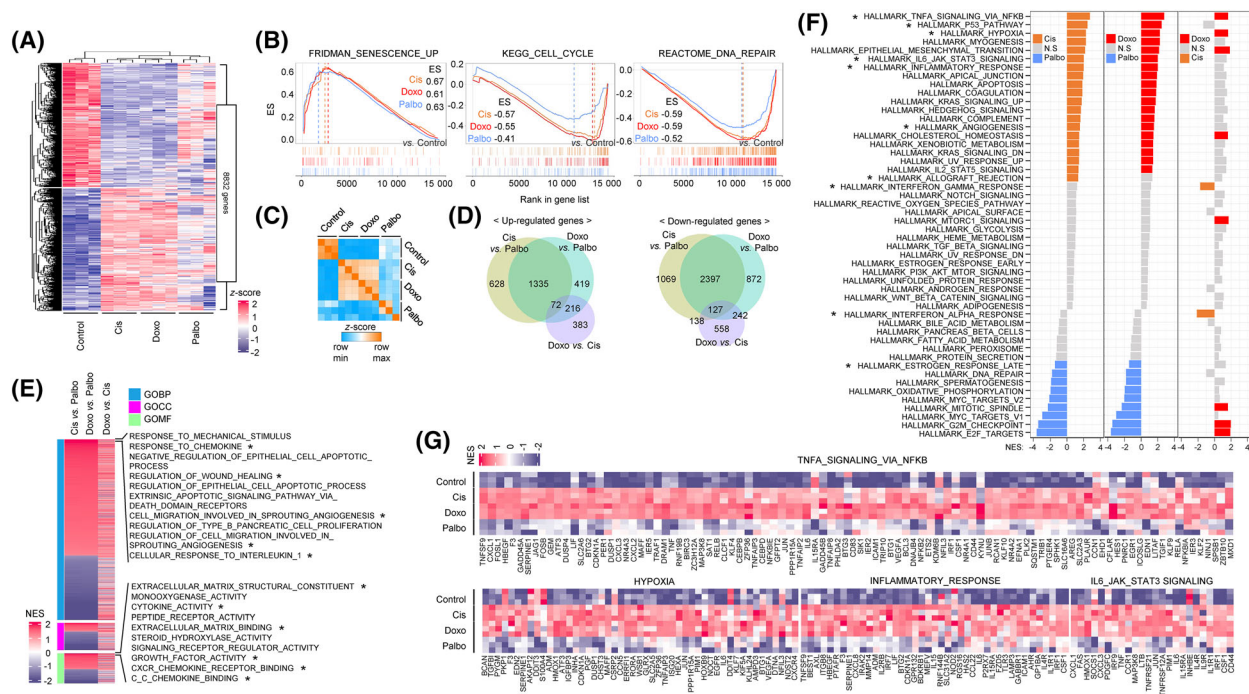


Fig. 2. Differential expression of genes related to pro-inflammatory response, anti-tumor immunity, and angiogenesis induced by DNA-damaging agents or CDK4/6i. (A) MCF-7 cells were treated with DNA-damaging agents (Cisplatin 5 μ M and Doxorubicin 100 nM) and CDK4/6i (Palbociclib 2 μ M) and RNA-seq analysis was performed after 5 days. A heatmap was generated from the whole transcriptome of control and senescent cells, showing a hierarchical clustering correlation with a z-score between the samples. Data are mean \pm SD of three ($N = 3$) independent experiments. (B) Overlapping GSEA plots showing representative senescent gene sets including senescence, cell cycle, and DNA repair, with ES, in TIS compared to the control. (C) A similarity index matrix of the whole transcriptome comparing TIS and control. The color bar indicates the z-score range, from the row min value to the row max value. (D) A Venn diagram showing significantly up- and downregulated genes between TIS groups. Light green: Cis vs. Palbo; sky blue: Doxo vs. Palbo; and purple: Doxo vs. Cis. (E) GO analysis of the whole transcriptome in TIS, presented as a heatmap. Significantly enriched top 10 gene sets indicated with an asterisk. (F) NES of HALLMARK gene sets in TIS are shown as a bar graph. Significantly enriched top 10 gene sets are indicated with an asterisk. (G) Heatmaps showing the leading edge of HALLMARK gene sets with z-score in the whole transcriptome. Cis, Cisplatin; Doxo, Doxorubicin; Palbo, Palbociclib.

transcriptome (Fig. 2A). The transcriptome analysis and GSEA of representative gene sets associated with general senescence showed that DNA-damaging agents- and CDK4/6i-induced senescence to a similar degree [24] (Fig. 2B). Despite the fact that all of the therapeutic agents altered expression of genes associated with TIS, we found differences in the expression patterns of genes induced by DNA-damaging agents and CDK4/6i (Fig. 2A). Pearson's correlation similarity matrix analysis showed highly similar transcriptome patterns in senescent cells induced by DNA-damaging agents, but global differences were observed between DNA-damaging agent- and CDK4/6i-induced senescence (Fig. 2C). Consistent with these results, the number of DEG between TIS by DNA-damage agents and CDK4/6i were significantly higher than that of DEG between TIS by DNA damage agents (Fig. 2D). To identify cellular processes related to the, respectively,

distinct patterns of gene expression in the senescence induced by different therapeutic agents, GSEA was performed with 33 591 gene sets (hallmark gene sets, curated gene sets, and ontology gene sets) as TIS vs. Control (Fig. S2). The gene ontology analysis with the comparison of TIS groups revealed that significantly distinctive cellular processes related to chemokines, angiogenesis, extracellular matrix structure, and cytokine activity were enriched in DNA-damaging agent-induced senescence (Fig. 2E). A 50 HALLMARK gene sets analysis revealed that gene sets potentially related to modulation of a pro-tumorigenic microenvironment (e.g., TNF/NF- κ B signaling, hypoxia, inflammatory responses, and angiogenesis) was significantly enriched in TIS with DNA-damaging agents compared to CDK4/6i. However, interestingly, NES of gene sets related to anti-tumorigenic immunity (e.g., allograft rejection, interferon-gamma responses,

and interferon-alpha responses) revealed no statistically significant difference between cells exposed to DNA-damaging agents and CDK4/6i (Fig. 2F). Heatmaps of the leading edge in the HALLMARK gene sets; TNF/NF- κ B signaling, hypoxia, inflammatory responses, and IL-6-JAK-STAT3 signaling, including well-known pro-inflammatory SASP (*CXCL1*, *CXCL2*, *CXCL3*, *CXCL8*, *CSFI*, *IL-6*, *PLAUR*, *TNF α* , and *VEGFA*), clearly showed a significant difference in gene expression profiles between cells in which senescence was induced by DNA-damaging agents and CDK4/6i (Fig. 2G). These findings suggest that although the two different groups of therapeutic agents induce senescence to a similar extent, they regulate genes associated with inflammatory response and angiogenesis in different ways. Therefore, DNA-damaging agent- and CDK4/6i-induced senescence has the potential to modulate the TME differently. To support our hypothesis, we conducted a comprehensive analysis of three types of modulators of the TME: SASP and ligands related to pro- and anti-tumorigenic immunity, and angiogenesis.

3.3. The pro-tumorigenic secretome and associated ligands are expressed at higher levels by DNA-damaging agent-induced senescent cancer cells than CDK4/6i-induced senescent cancer cells

To investigate the possibility of differential expression of secretome and ligands associated with pro-tumorigenic immune modulation by DNA-damaging agent- and CDK4/6i-induced senescent cancer cells, we performed GSEA using gene sets related to IL-6, TNF α , cytokines, and inflammation and showed that enrichment score (ES) of gene sets was significantly higher in the DNA-damaging agent- than in the CDK4/6i-induced senescent cells (Fig. 3A and Fig. S2A). The cnetplot of DNA-damaging agents vs. CDK4/6i showed that several pro-inflammatory SASP, including *CXCL1*, *CXCL3*, *CXCL8*, *IL-6*, *NF- κ B*, *TRAF1*, *TNF α* , and *TNFSF9*, were commonly upregulated among above gene sets (Fig. 3B). Although ES of the overlapping GSEA plot (HALLMARK_TNF_SIGNALING_VIA_NF-KB) in DNA-damaging agent-induced senescence was slightly higher than in CDK4/6i-induced senescence, the rank of representative pro-inflammatory and tumorigenic immune response genes was significantly higher in DNA-damaging agent-induced senescent cells (Fig. 3C). Consistent with the results from the above GSEA, the transcriptome data showed that expression of most secretory proteins and ligands associated with pro-

tumorigenic immune modulation which were categorized based on literature was upregulated in DNA-damaging agent-induced senescent cells than in CDK4/6i-induced senescent cells (Fig. 3D). Real-time qPCR further confirmed that transcripts of genes involved in the pro-tumorigenic immune response, such as TGF β family (*TGF β 1* and *TGF β 2*), inflammatory cytokines (*IL-6*, *TNF α*), neutrophil chemokines (*CXCL2*, *CXCL8*), macrophage M2 polarization inducers (*CSFI* and *ANXA1*), and NK and T-cell inhibitory ligands (*CEACAM1*, *CEACAM5*, *PVR*, and *CD274*), were more abundantly expressed in DNA-damaging agent-induced senescent cells (Fig. 3E). Protein levels of IL-6 and CXCL8 in conditioned medium from DNA-damaging agent-induced senescent cells were also significantly higher than in that from CDK4/6i-induced senescent cells (Fig. 3F). Taken together, these data indicate that DNA-damaging agent-induced senescence in breast cancer cells leads to more robust expression of various pro-inflammatory SASP (*TGF β 1*, *TGF β 2*, and *IL-6*, *CXCL2*, *CXCL8*, *CSFI*) and cell surface ligands (*CEACAM1*, *CEACAM5*, *PVR*, and *CD274*) that augment pro-tumorigenic immune responses within the TME.

3.4. Pro-angiogenic factors are more abundantly expressed by DNA-damaging agent-induced senescent cancer cells than by CDK4/6i-induced senescent cancer cells

Based on the finding that DNA-damaging agent-induced senescent cancer cells express high levels of VEGF (Fig. 2G), we investigated whether proteins secreted in the DNA-damaging agent-induced senescence are associated with angiogenesis. GSEA showed that gene sets related to angiogenesis, vascular endothelial cells, and hypoxia were significantly enriched in senescent cells induced by DNA-damaging agents (Fig. 4A and Fig. S2B). Among these gene sets, the commonly regulated genes were analyzed by cnetplot (Fig. 4B), revealing that the expression ranks of these genes were significantly lower in CDK4/6i-induced senescence (Fig. 4C). The heatmap of RNA-seq data for pro and anti-angiogenic factors revealed that levels of pro-angiogenic factors such as *VEGFA* [16], *HBEGF* [25,26], *PGF* [27], the *PDGF* family [28–31], and the *ANGPTL* family [32–36] were higher in DNA-damaging agent-induced senescent MCF-7 cells, while some anti-angiogenic factors were significantly upregulated in CDK4/6i-induced senescent cells (Fig. 4D). Real-time qPCR analysis demonstrated that expression of pro-angiogenic factors such as *VEGFA* and *GDF-15* [11,12,16] increased significantly in DNA-damaging

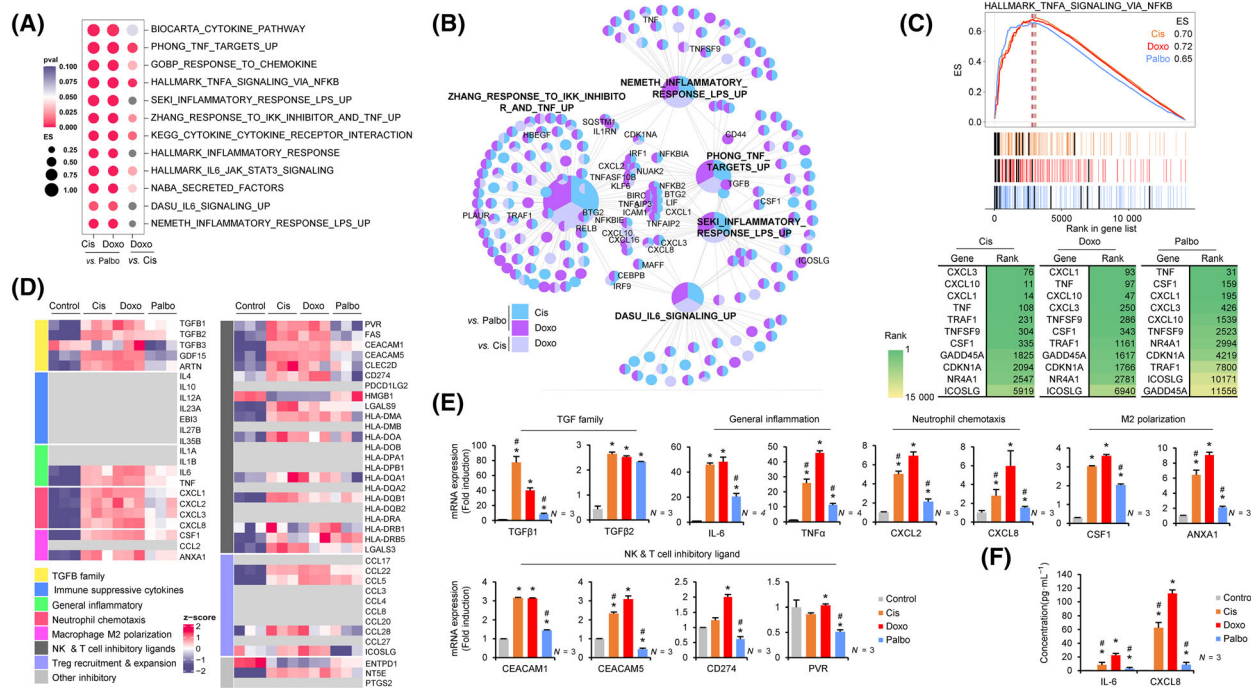


Fig. 3. Differential expression of pro-inflammatory SASP and ligands in DNA-damaging agent-induced senescent cancer cells compared to CDK4/6i-induced senescent cancer cells. (A) A comparison of enrichment score (ES) of pro-tumorigenic-related gene sets among TIS groups presented as a dotplot with P -value; Cis vs. Palbo, Doxo vs. Palbo, and Doxo vs. Cis. (B) A cnetplot of the gene sets selected from (A), showing significantly upregulated genes ($\log_2FC \geq 0.5$, $P \leq 0.05$) compared between the TIS groups; sky blue: Cis vs. Palbo; purple: Doxo vs. Palbo; and light purple: Doxo vs. Cis. The labeled genes on the cnetplot indicate pro-tumorigenic secretome, ligands, and cytokines belonging to each gene set. (C) An overlapping GSEA presenting ES (upper panel), rank in gene list (middle panel) between TIS vs. control. Indicated genes as black bars in the middle panel arranged in tabulated form based on their rank. The green gradient indicates the ranks of the genes (bottom panel). (D) A heatmap of pro-tumorigenic immune response-related SASP expression, generated from the transcriptome and presented with z-scores. The left panels of the heatmap indicate gene categories related to pro-tumorigenic immune response, and the gray in the heatmap indicates unexpressed genes. (E) MCF-7 cells were exposed to the DNA-damaging agents and CDK4/6i and harvested after 5 days. The expression levels of mRNA encoding representative SASP, chemokines, and ligands related to pro-tumorigenic immune responses were determined by RT-qPCR. Data are mean \pm SD of at least three ($N \geq 3$) independent experiments. The P -value was calculated using one-way ANOVA. * $P < 0.05$ (TIS vs. Control) and # $P < 0.05$ (Cis vs. Doxo, Palbo vs. Doxo). (F) The cells (4×10^5 cells/100 mm dish) were treated and harvested after 5 days. The concentrations ($\text{pg}\cdot\text{mL}^{-1}$) of IL-6 and CXCL8 were measured by ELISA in conditioned media collected from senescent and control cells. Data are mean \pm SD of three ($N = 3$) independent experiments. The P -value was calculated using one-way ANOVA. * $P < 0.05$ (TIS vs. Control) and # $P < 0.05$ (Cis vs. Doxo, Palbo vs. Doxo). Cis, Cisplatin; Doxo, Doxorubicin; Palbo, Palbociclib.

agent-induced senescent cells, whereas CDK4/6i-induced senescent cells showed significant upregulation of anti-angiogenic factors such as *COL4A3* [37,38], *MMRN2* [17], *TIMP1* [39], and *TIMP2* [40], along with a consistent trend toward the decreased expression of *VEGFA* (Fig. 4E). To confirm the reciprocal expression pattern of *VEGFA* mRNA as a master regulator of angiogenesis between DNA-damaging agent- and CDK4/6i-induced senescent cells, we measured the levels of VEGFA protein in a conditioned medium by ELISA. Consistent with mRNA expression data, the secretion level of VEGFA in conditioned medium from CDK4/6i-induced senescent cells was significantly lower than those in conditioned medium from non-senescent cells (Fig. 4F). Taken together, these findings

suggest that DNA-damaging agent-induced senescence can promote tumor angiogenesis via secretion of pro-angiogenic factors, while CDK4/6i-induced senescence can inhibit angiogenesis through regulation of anti-angiogenic factors in the TME.

3.5. The antigen presentation and interferon signaling activities of CDK4/6i-induced senescent cells are comparable with those of DNA-damaging agent-induced senescent cells

As shown in Fig. 2F, we did not find a significant difference in gene sets related to T-cell-mediated anti-tumor immunity between the TIS groups. This indicates that the capacity of CDK4/6i-induced senescence to

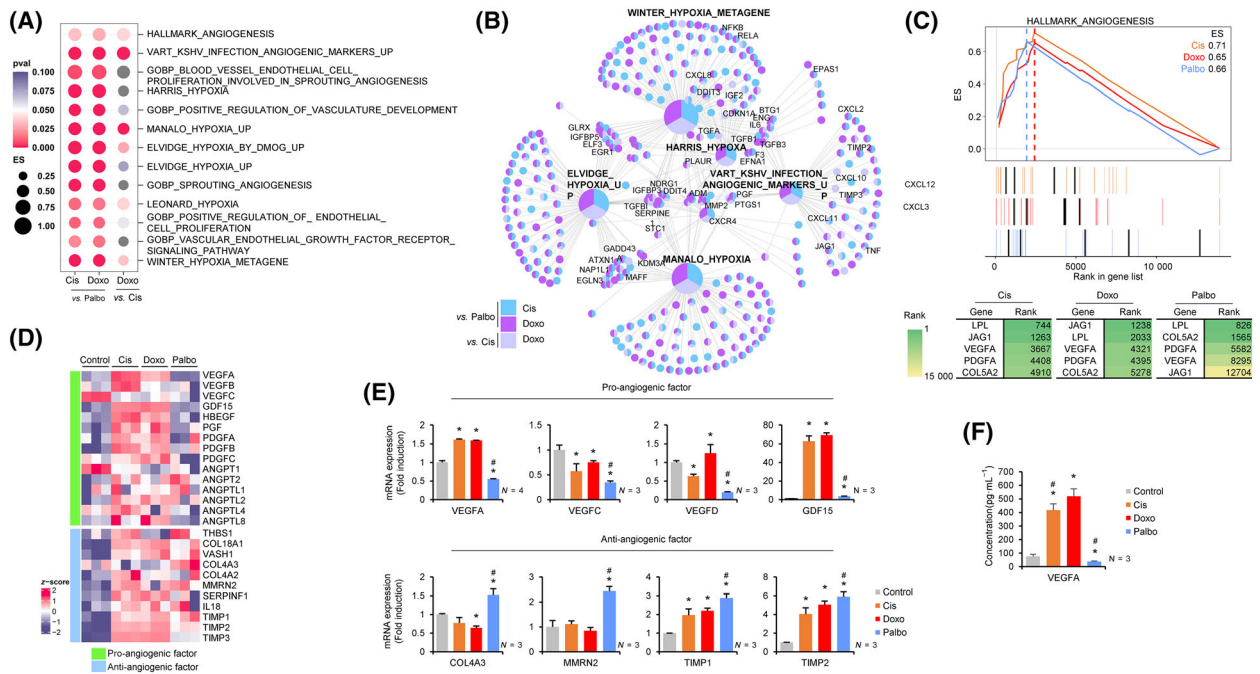


Fig. 4. Pro-angiogenic and anti-angiogenic factors are enriched in DNA-damaging agent- and CDK4/6i-induced senescent cells, respectively. (A) A comparison of enrichment score (ES) of pro-angiogenic gene sets among TIS groups presented as a dotplot with *P*-value; Cis vs. Palbo, Doxo vs. Palbo, and Doxo vs. Cis. (B) A cnetplot of the gene sets selected from (A), showing a comparison of the significantly up-regulated genes ($\log_2FC \geq 0.5, P \leq 0.05$) between TIS groups; sky blue: Cis vs. Palbo; purple: Doxo vs. Palbo; and light purple: Doxo vs. Cis. The labeled genes on the cnetplot indicate angiogenic factors belonging to each gene set. (C) An overlapping GSEA showing ES (upper panel) and rank in gene list (middle panel) between TIS vs. Control. Indicated genes are shown as black bars (middle panel) arranged in tabulated form based on rank. The green gradient indicates the ranks of the genes (bottom panel). (D) A heatmap of angiogenic factors was obtained from the transcriptome and presented as z-scores. The left panels of the heatmap indicate categories of pro- and anti-angiogenic factors, and the gray in the heatmap indicates unexpressed genes. (E) MCF-7 cells were treated with the agents and harvested after 5 days. The expression levels of pro-angiogenic and anti-angiogenic genes were determined by RT-qPCR. Data are mean \pm SD of at least three ($N = 3$) independent experiments. The *P*-value was calculated using one-way ANOVA. * $P < 0.05$ (TIS vs. Control) and # $P < 0.05$ (Cis vs. Doxo, Palbo vs. Doxo). (F) The cells (4×10^5 cells/100 mm dish) were treated and harvested after 5 days. The concentration (pg mL⁻¹) of VEGF was measured by ELISA in conditioned media collected from senescent and control cells. Data are mean \pm SD of three ($N = 3$) independent experiments. The *P*-value was calculated using one-way ANOVA. * $P < 0.05$ (TIS vs. Control) and # $P < 0.05$ (Cis vs. Doxo, Palbo vs. Doxo). Cis, Cisplatin; Doxo, Doxorubicin; Palbo, Palbociclib.

activate anti-tumor immunity is probably similar to that of DNA-damaging agent-induced senescence, despite the reduced secretion of pro-inflammatory and pro-angiogenic SASP in the CDK4/6i-group. GSEA analysis of gene sets related to allograft rejection, T-cell-mediated cytotoxicity, and antigen presentation revealed no statistical differences between the therapeutic agents, supporting the above observations (Fig. 5A and Fig. S2C). The cnetplot with above gene sets revealed that senescent cancer cells induced by all three agents increased expression of antigen presentation factors (Fig. 5B). Moreover, the overlapping GSEA showed that the rank of genes related to antigen presentation (*HLA-F*, *HLA-B*, *HLA-C*, *TAP1*, and *B2M*) [41–47] in the CDK4/6i-group was slightly higher compared to that in the DNA-damaging agent group (Fig. 5C). The heatmap for genes involved

in activating anti-tumor immune responses showed increased expression of T-cell chemokines (*CXCL9*, *CXCL10*, and *CXCL11*) [48–52], antigen processing proteins (*TAP1*, *TAP2*, *TAPBP*, *ERAP1*, and *ERAP2*) [44,45,53–56], and MHC class I molecules (*HLAs* and *B2M*) in both DNA-damaging agent- and CDK4/6i-induced senescent cells, indicating activation of anti-tumor immunity in both the groups (Fig. 5D). These results are consistent with those of recent studies [57,58]. To validate the RNA-seq results for anti-tumor immunity, we performed RT-qPCR on independent experimental samples to detect representative genes (Fig. 5E). Consistent with RNA-seq data, all three types of senescent cancer cells showed increased expression of genes related to anti-tumor immunity. Interestingly, increased expression of *CXCL9*, *CXCL10*, *CXCL11*, *MICB*,

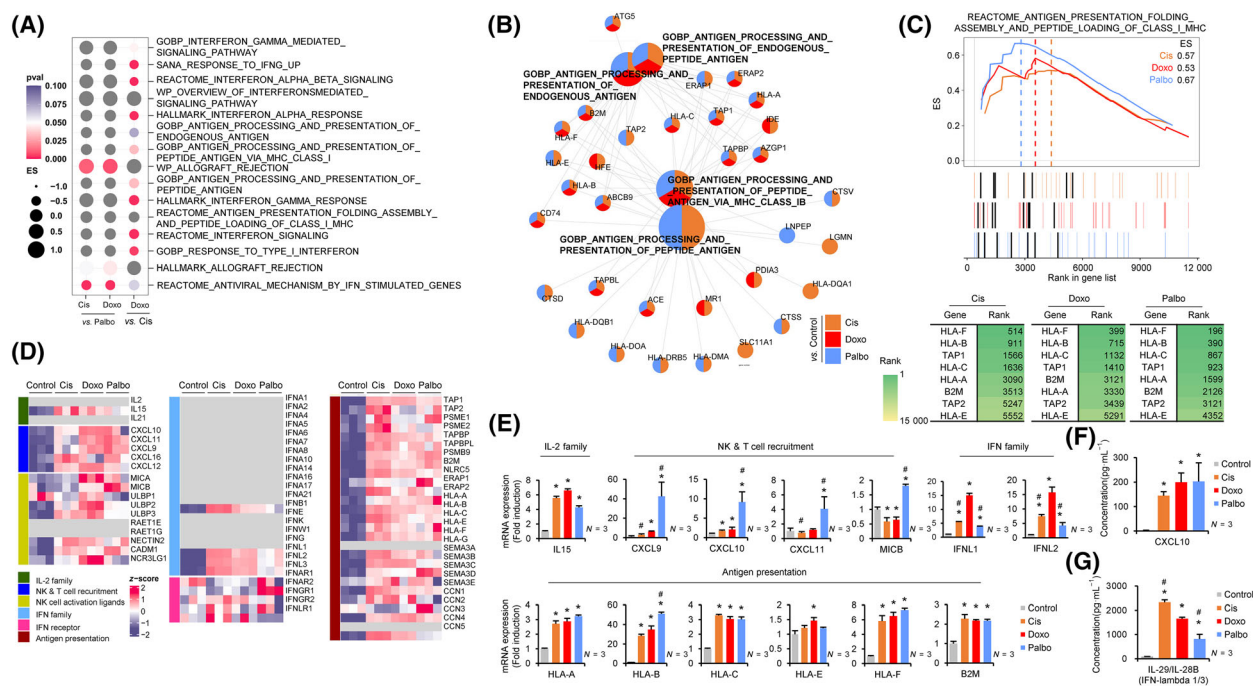


Fig. 5. A similar antigen presentation and interferon signaling activities in DNA-damaging agent- and CDK4/6i-induced senescent cells. (A) A comparison of ES of anti-tumorigenic immune response-related gene sets among TIS groups with P -value; Cis vs. Palbo, Doxo vs. Palbo, and Doxo vs. Cis. (B) A cnetplot of the gene sets selected from (A), showing a comparison of the significantly upregulated genes ($\log_2FC \geq 0.5$, $P \leq 0.05$) of TIS groups vs. Control; orange: Cis vs. Control; red: Doxo vs. Control; and blue: Doxo vs. Control. The labeled genes in the cnetplot indicate genes associated with antigen presentation within each gene set. (C) An overlapping GSEA showing ES (upper panel), rank in gene list (middle panel) between TIS vs. Control. Indicated genes as black bars (middle panel) arranged in tabulated form based on their rank. The green gradient indicates the ranks of the genes (bottom panel). (D) A heatmap of anti-tumorigenic immune response factors was obtained from the transcriptome and presented as z -scores. The left panels of the heatmap indicate the categories of anti-tumorigenic immune response factors, and the gray in the heatmap indicates unexpressed genes. (E) MCF-7 cells were treated with the agents and harvested after 5 days. The expression levels of anti-tumorigenic were determined by RT-qPCR. Data are mean \pm SD of three ($N = 3$) independent experiments. The P -value was calculated by the one-way ANOVA. * $P < 0.05$ (TIS vs. Control) and # $P < 0.05$ (Cis vs. Doxo, Palbo vs. Doxo). (F, G) The cells (4×10^5 cells/100 mm dish) were treated and harvested after 5 days. The concentrations ($\text{pg}\cdot\text{mL}^{-1}$) of CXCL10 and IFN- λ were measured by ELISA in conditioned media collected from senescent and control cells. Data are mean \pm SD of three ($N = 3$) independent experiments. The P -value was calculated using one-way ANOVA. * $P < 0.05$ (TIS vs. Control) and # $P < 0.05$ (Cis vs. Doxo, Palbo vs. Doxo). Cis, Cisplatin; Doxo, Doxorubicin; Palbo, Palbociclib.

HLA-B, and *HLA-F* was more pronounced in CDK4/6i-induced senescent cells than in DNA-damaging agent-induced senescent cells. Consistent with the mRNA data, the CXCL10 protein level in the conditioned medium derived from CDK4/6i-induced senescence exhibited comparable or slightly elevated levels in comparison with DNA-damaging agent-induced senescence. IFN signaling activates downstream target genes involved in antigen presentation [49,59,60] as well as expression of T-cell chemokines [61,62]. Previous studies demonstrate that intracellular antiviral defense mechanisms could be triggered during cellular senescence through endogenous retroviral activation, resulting in IFN expression [63,64]. Transcriptome analysis revealed no marked expression of basal mRNA transcripts of IFN- α and IFN- γ in MCF-7 cells, with no increase

observed after TIS. However, there was a significant increase in mRNA transcripts of IFN- β (*IFNB1*) and IFN- λ (*IFNL1*, *IFNL2*, and *IFNL3*) by TIS. Furthermore, the secreted protein level of IFN- λ in conditioned medium from senescent cells was significantly higher than that in conditioned medium from non-senescent cells (Fig. 5F). These findings suggest that TIS triggers the expression of genes related to anti-tumor immune activation. CDK4/6i-induced senescence also has this ability, at levels comparable to or even greater than that of DNA-damaging agents.

For further confirmation of the above observations from MCF-7 cells, another breast cancer cell line, HCC1428 (HR: positive/HER2: negative) [65], was used for TIS by DNA-damaging agents and CDK4/6i. Similar to MCF-7, SA- β -gal activity (Fig. S3A) and

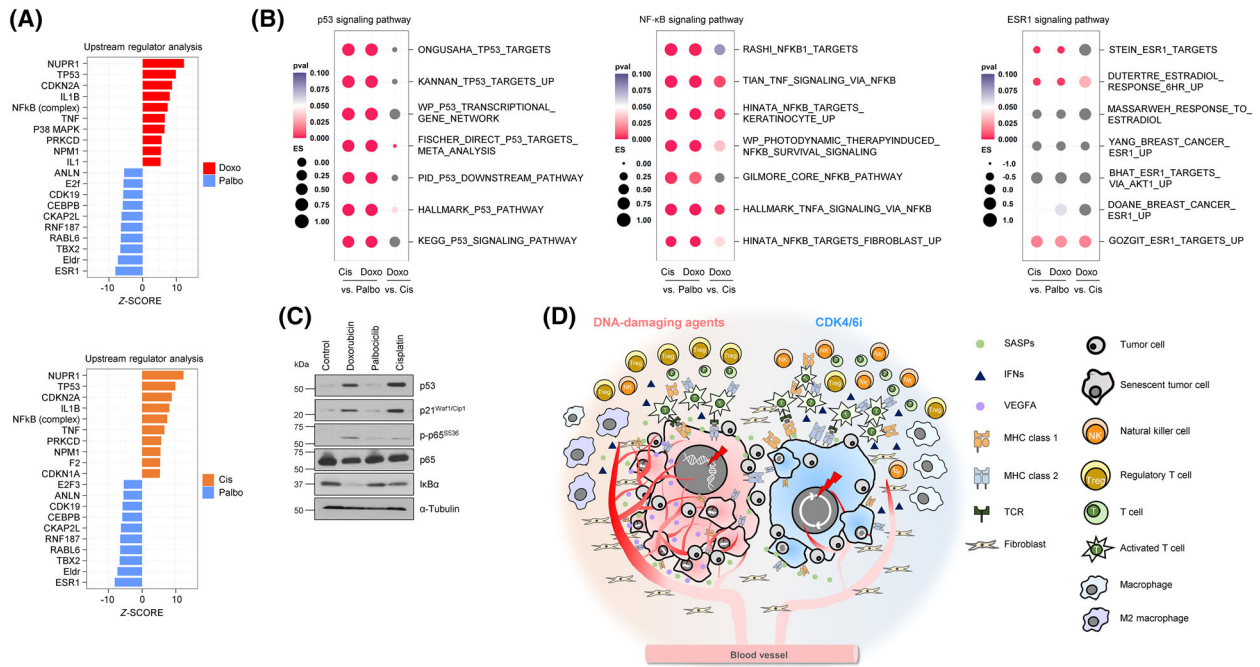


Fig. 6. Exclusive activation of p53 and NF-κB signaling in DNA-damaging agent-induced senescent cells. (A) IPA was performed to analyze upstream regulators and their expression levels were compared between TIS groups; Doxo vs. Palbo and Cis vs. Palbo. The top 10 regulators were ranked according to the z-score with $P \leq 0.05$. (B) A comparison of ES of p53, NF-κB, and ESR1 signaling-related gene sets among TIS groups with P -value; Cis vs. Palbo, Doxo vs. Palbo, and Doxo vs. Cis. (C) MCF-7 cells were treated with DNA-damaging agents and CDK4/6i and harvested after 5 days. The p53, p21^{Waf1/Cip1} expression, and NF-κB activation were determined by immunoblotting. α-tubulin was used as a loading control. Data are representative of three ($N = 3$) independent experiments. (D) An illustration depicting the effect of DNA-damaging agents and CDK4/6i-induced senescence on the TME of breast cancer cells. Cis, Cisplatin; Doxo, Doxorubicin; Palbo, Palbociclib.

reduced expression of E2F target genes (Fig. S3B) showed that a comparable extent of senescence was induced by different types of agents. Increased phosphorylation of γH2AX was also observed only in senescent cells induced by DNA-damaging agents (Fig. S3C). Increased phosphorylation of c-Jun, Erk1/2, STAT3, and AKT after TIS and slightly stronger phosphorylation of STAT3 in CDK4/6i-induced senescent cells compared to those of DNA-damaging agent-induced senescent cells was also observed in HCC1428 cells (Fig. S3D). In HCC1428 cells, DNA-damaging agent-induced senescence showed higher mRNA (Fig. S3E,G) and protein levels (Fig. S3H) of pro-inflammatory SASP (*TGFβ1*, *IL-6*, *CXCL8*, and *ANXA1*) and pro-angiogenic factors (*VEGFA*, *VEGFB*, and *GDF15*) compared to those of CDK4/6i-induced senescence. While consistent with data from MCF-7, the expression level of genes related to anti-tumor immunity such as T-cell chemokines (*CXCL9*, *CXCL10*, and *CXCL11*) and antigen presentation (*HLAs* and *B2M*) in CDK4/6i-induced senescent cells is similar or even higher than those of DNA-damaging

agent-induced senescent cells (Fig. S3G), consistent with the mRNA data, in HCC1428, *CXCL10* and *IFN-λ* protein level in the conditioned medium derived from CDK4/6i-induced senescence was also higher than those of DNA-damaging agent-induced senescence (Fig. S3H). In addition, senescent cancer cells by other types of DNA damaging agents (Etoposide and Carboplatin) (Fig. S4A,B) and CDK4/6i (Abemaciclib) also showed similar trends of mRNA expression pattern in pro-inflammatory SASP (Fig. S4C), pro-angiogenic factors (Fig. S4D), and anti-tumor immune-related genes (Fig. S4F).

3.6. DNA-damaging agent-induced senescence activates p53 and NF-κB signaling significantly more strongly than CDK4/6i-induced senescence

Since the transcriptome analysis demonstrated a definitive difference between DNA-damaging agent- and CDK4/6i-induced senescence, we wonder if the presence of distinct upstream regulators can be expected by IPA. *TP53* and *NF-κB* complex were enriched in

DNA-damaging agents, while estrogen receptor (*ESR1*) was enriched in CDK4/6i (Fig. 6A). The presence of these expected upstream regulators was supported by dotplot of gene sets associated with *TP53*, *TNF/NF-κB*, and *ESR1* (Fig. 6B, Fig. S5). The strong stabilization of p53, expression of p21^{Waf1/Cip1}, phosphorylation of p65, and degradation of IκB, which were observed only in DNA-damaging agent-induced senescent cells, supported the results of IPA analysis in MCF-7 and HCC1428 cell lines (Fig. 6C, Fig. S31). Therefore, considering that DNA damage response can activate NF-κB signaling [66,67], somewhat exclusive p53 and NF-κB activation in DNA-damaging agent-induced senescence could explain the robust expression of pro-inflammatory and pro-angiogenic proteins. These results suggest that p53 and NF-κB are not essential transcription factors for the expression of anti-tumor immune-related proteins in TIS.

4. Discussion

In the present study, although the extent of senescence elicited by DNA-damaging agents and CDK4/6i was similar, CDK4/6i-induced senescent cancer cells showed significantly lower expression of well-known pro-inflammatory SASP such as *IL-6*, *CXCL1*, *CXCL8*, and *TGF-β*. In a previous study, Coppe et al. demonstrated that overexpression of p16^{INK4A} induces premature cellular senescence without expression of SASP [18]. However, unlike the results of Coppe et al., other studies showed that CDK4/6i-induced senescent cells expressed various SASP. Guan et al. observed that CDK4/6i (Palbociclib)-induced senescent MEFs exhibited a more robust pro-inflammatory gene expression profile than fibroblasts triggered to enter senescence by exposure to UV light or MMC; in addition, there was no DNA damage and p53 activation [19]. By contrast, Wang et al. demonstrated that CDK4/6i-induced senescence in BJ fibroblasts was dependent on p53 activity, with no increase of NF-κB activity or NF-κB-driven SASP molecules such as *IL-6*, *CXCL1*, or *CCL5* [68]. However, in contrast with Wang et al study [68], we found increased expression of γH2AX and p21^{Waf1/Cip1} proteins, and strong enrichment of gene sets related to p53 activation, in cells exposed to DNA-damaging agents only. Therefore, our results clearly suggest that CDK4/6i elicit cancer cell senescence without robust DNA damage or activation of p53 signaling. Since several studies show that DNA damage signals can activate NF-κB and vice versa [67,69], the stronger expression of a pro-inflammatory SASP can be explained, in part, by NF-κB activation by DNA-damaging agents.

Increased expression of VEGF is a common characteristic of senescent human and mouse fibroblasts [18]. A recent study showed that combined treatment of a MAPK inhibitor (Trametinib) and Palbociclib induced senescence and these senescent pancreatic ductal adenocarcinoma cells showed increased secretion of pro-angiogenic factors (VEGF, PDGFA/B, and FGF2) and MMPs (MMP2/3/7/9/10) [70]. However, in the present study, CDK4/6i-induced senescence showed a decrease in VEGF expression. In addition, expression of other pro-angiogenic factors was significantly lower in senescent breast cancer cells induced by CDK4/6i, whereas DNA-damaging agent-induced senescence increased expression of pro-tumorigenic factors, including VEGF. Therefore, TIS after chemotherapy with conventional genotoxic agents may augment the survival and progression of non-senescent residual cancer cells by promoting angiogenesis. In addition, considering the role of VEGF in inhibiting anti-tumor immunity, senescent cancer cells induced by DNA-damaging agents can promote a more potent pro-tumorigenic immune microenvironment than CDK4/6i. Nevertheless, while some studies suggest that pro-inflammatory and pro-angiogenic SASP can enhance immune surveillance by NK cells [71], and improve the delivery of chemotherapeutic drugs [70], respectively, more research is needed to determine which types of chemotherapeutic agents (DNA-damaging agents vs. CDK4/6i) can induce cancer cell senescence with more robust anti-tumor immunomodulating capabilities.

If all the features of CDK4/6i-induced senescence are less potent than those of DNA-damaging agents, the implications of this study may not be significant. The most interesting point of this study is that CDK4/6i-induced senescence still maintains the expression of SASP and ligands associated with anti-tumor immunity. To elicit robust anti-tumor immune responses, proper recruitment and tumor recognition of cytotoxic T cells are important. During CDK4/6i-induced TIS, expression of genes related to antigen processing and presentation by MHC-I (*HLA*, *B2M*, *TAP1*, and *ERAP1*), and those related to chemokines involved in T-cell chemotaxis (*CXCL9*, *10*, *11*), was similar or even higher in senescence induced by CDK4/6i than DNA damaging agents. The results of a recent study showed that induction of senescence in cancer cells by various agents (Doxorubicin, Palbociclib, and Nutlin-3A) increased expression of classical MHC-I family and genes related to antigen processing [57] are consistent with our results. In addition, to the best of our knowledge, this is the first report to show that processes related to antigen presentation and T-cell

chemokine expression are activated more strongly by senescence induced by CDK4/6i than by senescence induced by DNA-damaging agents.

According to our findings, activation of the NF- κ B pathway, as indicated by the phosphorylation of NF- κ B and the degradation of I κ B α , was more prominent in senescent cells induced by DNA-damaging agents. Conversely, the activation of STAT3, as assessed by its phosphorylation status, was comparatively higher in senescent cells induced by CDK4/6i. The differential activation of these signaling pathways could explain the distinct expression patterns of SASP and ligands induced by DNA-damaging agents and CDK4/6i. The concept suggested by previous studies showing that pro- and anti-tumorigenic SASP can be regulated separately by different signal pathways [72] can be applied to the results of the present study, although further studies are needed to identify which signal pathway is the main regulator for anti-tumorigenic immunity during TIS.

Recent studies have shown that senescent cancer cells are highly immunogenic, and that immunization with senescent cancer cells [19], or nanovesicles [73] secreted by these cells, elicits strong anti-tumor immune surveillance. From this point of view, further research comparing the induction of cancer cell senescence by different agents, and identifying the most potent immunogenic senescence inducers, will facilitate the development of more powerful therapeutic cancer vaccines based on senescent cancer cells. Nonetheless, experiments with mouse models, and analysis of human cancer samples treated with the above agents, need to be performed to validate our observation that DNA-damaging agents and CDK4/6i-induced senescence could have the potential to regulate the TME in different ways. Moreover, CDK4/6i are typically administered in conjunction with anti-hormonal therapy, such as AI, in clinical practice for breast cancer treatment. Therefore, our results do not exclude the possibility that the reduced estrogen levels following AI treatment could influence the process of TIS by CDK4/6i in the cancer tissue of patients. Additionally, it should be noted that the results of the current study are limited to HR-positive and HER2-negative breast cancer cells and may need to be extended to other types of tumors.

5. Conclusion

We show that the SASP composition is highly dependent on the type of senescence inducer. CDK4/6i-induced senescent cancer cells clearly showed less prominent expression of SASP and ligands associated with

inflammation and angiogenesis, while comparable or even higher expression of SASP and ligands associated with anti-tumor immunity compared to DNA-damaging agent-induced senescent cancer cells. These differences can elicit more favorable TME for cancer immune surveillance, potentially leading to better treatment outcomes (Fig. 6D). Taken together, our study provides a framework for a better understanding of TME modulation by TIS and may offer valuable insights into designing more effective senescence inducers as a therapeutic strategy.

Acknowledgements

The authors are grateful to the National Research Foundation of the Republic of Korea and the Ministry of Health & Welfare, Republic of Korea for financial support. This study was supported by grants from the National Research Foundation of the Republic of Korea to Tae Jun Park at Ajou University (NRF-2019R1A2C2086127, NRF-2020R1A6A1A03043539, NRF-2020M3A9D8037604), and by National Research Foundation of Korea and by the Korea Health Technology R&D Project through the Korea Health Industry Development Institute, funded by the Ministry of Health & Welfare, Republic of Korea to Yong Won Choi (NRF-2021R1C1C1012266, HR22C1734).

Conflict of interest

The authors declare no conflict of interest.

Author contributions

DHL and MI performed the experiments, analyzed the data, and wrote the manuscript; JHC, YJP YHK, and SM participated in experiments and data interpretation; TJP and YWC designed the study, involved in supervision, project administration, interpretation, editing, and funding acquisition. All authors approved the final version of the manuscript.

Peer review

The peer review history for this article is available at <https://www.webofscience.com/api/gateway/wos/peer-review/10.1002/1878-0261.13541>.

Data accessibility

The data analyzed in this study are included either in this article or in additional files. Datasets for RNA-seq have been deposited in GEO under accession No.

GSE229264. <https://www.ncbi.nlm.nih.gov/geo/query/acc.cgi?acc=GSE229264>.

References

- Schmitt CA, Fridman JS, Yang M, Lee S, Baranov E, Hoffman RM, et al. A senescence program controlled by p53 and p16INK4a contributes to the outcome of cancer therapy. *Cell*. 2002;**109**:335–46.
- Laine A, Sihto H, Come C, Rosenfeldt MT, Zwolinska A, Niemela M, et al. Senescence sensitivity of breast cancer cells is defined by positive feedback loop between CIP2A and E2F1. *Cancer Discov*. 2013;**3**:182–97.
- Hinds P, Pietruska J. Senescence and tumor suppression. *F1000Res*. 2017;**6**:2121.
- Was H, Czarnecka J, Kominek A, Barszcz K, Bernas T, Piwocka K, et al. Some chemotherapeutics-treated colon cancer cells display a specific phenotype being a combination of stem-like and senescent cell features. *Cancer Biol Ther*. 2018;**19**:63–75.
- Mongiardi MP, Pellegrini M, Pallini R, Levi A, Falchetti ML. Cancer response to therapy-induced senescence: a matter of dose and timing. *Cancers*. 2021;**13**:484.
- Tato-Costa J, Casimiro S, Pacheco T, Pires R, Fernandes A, Alho I, et al. Therapy-induced cellular senescence induces epithelial-to-mesenchymal transition and increases invasiveness in rectal cancer. *Clin Colorectal Cancer*. 2016;**15**:170–178.e3.
- Tonnessen-Murray CA, Frey WD, Rao SG, Shahbandi A, Ungerleider NA, Olayiwola JO, et al. Chemotherapy-induced senescent cancer cells engulf other cells to enhance their survival. *J Cell Biol*. 2019;**218**:3827–44.
- Choi YW, Kim YH, Oh SY, Suh KW, Kim YS, Lee GY, et al. Senescent tumor cells build a cytokine shield in colorectal cancer. *Adv Sci*. 2021;**8**:2002497.
- Demaria M, O'Leary MN, Chang J, Shao L, Liu S, Alimirah F, et al. Cellular senescence promotes adverse effects of chemotherapy and cancer relapse. *Cancer Discov*. 2017;**7**:165–76.
- Coppe JP, Desprez PY, Krtolica A, Campisi J. The senescence-associated secretory phenotype: the dark side of tumor suppression. *Annu Rev Pathol*. 2010;**5**:99–118.
- Wang Z, He L, Li W, Xu C, Zhang J, Wang D, et al. GDF15 induces immunosuppression via CD48 on regulatory T cells in hepatocellular carcinoma. *J Immunother Cancer*. 2021;**9**:e002787.
- Bourhis M, Palle J, Galy-Fauroux I, Terme M. Direct and indirect modulation of T cells by VEGF-A counteracted by anti-angiogenic treatment. *Front Immunol*. 2021;**12**:616837.
- Ma Y, Liu Y, Zhi Y, Wang H, Yang M, Niu J, et al. Delivery of CXCL9/10/11 plasmid DNAs promotes the tumor-infiltration of T cells and synergizes with PD1 antibody for treating lung cancer. *Cancer Nanotechnol*. 2022;**13**:1–13.
- Ferrari de Andrade L, Kumar S, Luoma AM, Ito Y, Alves da Silva PH, Pan D, et al. Inhibition of MICA and MICB shedding elicits NK-cell-mediated immunity against tumors resistant to cytotoxic T cells. *Cancer Immunol Res*. 2020;**8**:769–80.
- Ross SH, Cantrell DA. Signaling and function of interleukin-2 in T lymphocytes. *Annu Rev Immunol*. 2018;**36**:411–33.
- Nyberg P, Salo T, Kalluri R. Tumor microenvironment and angiogenesis. *Front Biosci*. 2008;**13**:6537–53.
- Lorenzon E, Colladel R, Andreuzzi E, Marastoni S, Todaro F, Schiappacassi M, et al. MULTIMERIN2 impairs tumor angiogenesis and growth by interfering with VEGF-A/VEGFR2 pathway. *Oncogene*. 2012;**31**:3136–47.
- Coppe JP, Kauser K, Campisi J, Beausejour CM. Secretion of vascular endothelial growth factor by primary human fibroblasts at senescence. *J Biol Chem*. 2006;**281**:29568–74.
- Guan X, LaPak KM, Hennessey RC, Yu CY, Shakya R, Zhang J, et al. Stromal senescence by prolonged CDK4/6 inhibition potentiates tumor growth. *Mol Cancer Res*. 2017;**15**:237–49.
- Yoshida A, Lee EK, Diehl JA. Induction of therapeutic senescence in Vemurafenib-resistant melanoma by extended inhibition of CDK4/6. *Cancer Res*. 2016;**76**:2990–3002.
- Lelliott EJ, Kong IY, Zethoven M, Ramsbottom KM, Martelotto LG, Meyran D, et al. CDK4/6 inhibition promotes antitumor immunity through the induction of T-cell memory. *Cancer Discov*. 2021;**11**:2582–601.
- Goel S, DeCristo MJ, Watt AC, BrinJones H, Sceneay J, Li BB, et al. CDK4/6 inhibition triggers anti-tumour immunity. *Nature*. 2017;**548**:471–5.
- Deng J, Wang ES, Jenkins RW, Li S, Dries R, Yates K, et al. CDK4/6 inhibition augments antitumor immunity by enhancing T-cell activation. *Cancer Discov*. 2018;**8**:216–33.
- Deschênes-Simard X, Roy S, Ferbeyre G. Genome reprogramming in cells that escape from senescence. *Bionatura*. 2016;**1**:54–61.
- Mehta VB, Besner GE. HB-EGF promotes angiogenesis in endothelial cells via PI3-kinase and MAPK signaling pathways. *Growth Factors*. 2007;**25**:253–63.
- Ongusaha PP, Kwak JC, Zwible AJ, Macip S, Higashiyama S, Taniguchi N, et al. HB-EGF is a potent inducer of tumor growth and angiogenesis. *Cancer Res*. 2004;**64**:5283–90.
- Carmeliet P, Moons L, Luttun A, Vincenti V, Compernelle V, De Mol M, et al. Synergism between vascular endothelial growth factor and placental growth factor contributes to angiogenesis and plasma

- extravasation in pathological conditions. *Nat Med*. 2001;**7**:575–83.
- 28 Cao R, Brakenhielm E, Li X, Pietras K, Widenfalk J, Ostman A, et al. Angiogenesis stimulated by PDGF-CC, a novel member in the PDGF family, involves activation of PDGFR- α and - β receptors. *FASEB J*. 2002;**16**:1575–83.
 - 29 Chen J, Yuan W, Wu L, Tang Q, Xia Q, Ji J, et al. PDGF-D promotes cell growth, aggressiveness, angiogenesis and EMT transformation of colorectal cancer by activation of Notch1/Twist1 pathway. *Oncotarget*. 2017;**8**:9961–73.
 - 30 Hosaka K, Yang Y, Nakamura M, Andersson P, Yang X, Zhang Y, et al. Dual roles of endothelial FGF-2-FGFR1-PDGFB and perivascular FGF-2-FGFR2-PDGFR β signaling pathways in tumor vascular remodeling. *Cell Discov*. 2018;**4**:3.
 - 31 Shikada Y, Yonemitsu Y, Koga T, Onimaru M, Nakano T, Okano S, et al. Platelet-derived growth factor-AA is an essential and autocrine regulator of vascular endothelial growth factor expression in non-small cell lung carcinomas. *Cancer Res*. 2005;**65**:7241–8.
 - 32 Chen E, Tang C, Peng K, Cheng X, Wei Y, Liu T. ANGPTL6-mediated angiogenesis promotes alpha fetoprotein-producing gastric cancer progression. *Pathol Res Pract*. 2019;**215**:152454.
 - 33 Oike Y, Yasunaga K, Suda T. Angiopoietin-related/angiopoietin-like proteins regulate angiogenesis. *Int J Hematol*. 2004;**80**:21–8.
 - 34 Parri M, Pietrovito L, Grandi A, Campagnoli S, De Camilli E, Bianchini F, et al. Angiopoietin-like 7, a novel pro-angiogenic factor over-expressed in cancer. *Angiogenesis*. 2014;**17**:881–96.
 - 35 Xie JY, Wei JX, Lv LH, Han QF, Yang WB, Li GL, et al. Angiopoietin-2 induces angiogenesis via exosomes in human hepatocellular carcinoma. *Cell Commun Signal*. 2020;**18**:46.
 - 36 Zhong L, Tang L, He X. Angiopoietin-like 3 (ANGPTL3) drives cell proliferation, migration and angiogenesis in cervical cancer via binding to integrin α v β 3. *Bioengineered*. 2022;**13**:2971–80.
 - 37 Hamano Y, Zeisberg M, Sugimoto H, Lively JC, Maeshima Y, Yang C, et al. Physiological levels of tumstatin, a fragment of collagen IV α 3 chain, are generated by MMP-9 proteolysis and suppress angiogenesis via α v β 3 integrin. *Cancer Cell*. 2003;**3**:589–601.
 - 38 Mundel TM, Kalluri R. Type IV collagen-derived angiogenesis inhibitors. *Microvasc Res*. 2007;**74**:85–9.
 - 39 Reed MJ, Koike T, Sadoun E, Sage EH, Puolakkainen P. Inhibition of TIMP1 enhances angiogenesis in vivo and cell migration in vitro. *Microvasc Res*. 2003;**65**:9–17.
 - 40 Seo DW, Li H, Guedez L, Wingfield PT, Diaz T, Salloum R, et al. TIMP-2 mediated inhibition of angiogenesis: an MMP-independent mechanism. *Cell*. 2003;**114**:171–80.
 - 41 Lin A, Yan WH. The emerging roles of human leukocyte antigen-F in immune modulation and viral infection. *Front Immunol*. 2019;**10**:964.
 - 42 Huang J, Goedert JJ, Sundberg EJ, Cung TD, Burke PS, Martin MP, et al. HLA-B*35-Px-mediated acceleration of HIV-1 infection by increased inhibitory immunoregulatory impulses. *J Exp Med*. 2009;**206**:2959–66.
 - 43 Papuchova H, Meissner TB, Li Q, Strominger JL, Tilburgs T. The dual role of HLA-C in tolerance and immunity at the maternal-fetal interface. *Front Immunol*. 2019;**10**:2730.
 - 44 Ritz U, Seliger B. The transporter associated with antigen processing (TAP): structural integrity, expression, function, and its clinical relevance. *Mol Med*. 2001;**7**:149–58.
 - 45 Agrawal S, Reemtsma K, Bagiella E, Oluwole SF, Braunstein NS. Role of TAP-1 and/or TAP-2 antigen presentation defects in tumorigenicity of mouse melanoma. *Cell Immunol*. 2004;**228**:130–7.
 - 46 Zhao Y, Cao Y, Chen Y, Wu L, Hang H, Jiang C, et al. B2M gene expression shapes the immune landscape of lung adenocarcinoma and determines the response to immunotherapy. *Immunology*. 2021;**164**:507–23.
 - 47 Wang C, Wang Z, Yao T, Zhou J, Wang Z. The immune-related role of beta-2-microglobulin in melanoma. *Front Oncol*. 2022;**12**:944722.
 - 48 Gao Q, Wang S, Chen X, Cheng S, Zhang Z, Li F, et al. Cancer-cell-secreted CXCL11 promoted CD8(+) T cells infiltration through docetaxel-induced-release of HMGB1 in NSCLC. *J Immunother Cancer*. 2019;**7**:42.
 - 49 Huang H, Zhou W, Chen R, Xiang B, Zhou S, Lan L. CXCL10 is a tumor microenvironment and immune infiltration related prognostic biomarker in pancreatic adenocarcinoma. *Front Mol Biosci*. 2021;**8**:611508.
 - 50 Li Y, Han S, Wu B, Zhong C, Shi Y, Lv C, et al. CXCL11 correlates with immune infiltration and impacts patient immunotherapy efficacy: a Pan-cancer analysis. *Front Immunol*. 2022;**13**:951247.
 - 51 Liang YK, Deng ZK, Chen MT, Qiu SQ, Xiao YS, Qi YZ, et al. CXCL9 is a potential biomarker of immune infiltration associated with favorable prognosis in ER-negative breast cancer. *Front Oncol*. 2021;**11**:710286.
 - 52 Zumwalt TJ, Arnold M, Goel A, Boland CR. Active secretion of CXCL10 and CCL5 from colorectal cancer microenvironments associates with GranzymeB+ CD8+ T-cell infiltration. *Oncotarget*. 2015;**6**:2981–91.
 - 53 Andres AM, Dennis MY, Kretschmar WW, Cannons JL, Lee-Lin SQ, Hurle B, et al. Balancing selection maintains a form of ERAP2 that undergoes nonsense-mediated decay and affects antigen presentation. *PLoS Genet*. 2010;**6**:e1001157.

- 54 York IA, Brehm MA, Zendzian S, Towne CF, Rock KL. Endoplasmic reticulum aminopeptidase 1 (ERAP1) trims MHC class I-presented peptides in vivo and plays an important role in immunodominance. *Proc Natl Acad Sci U S A*. 2006;**103**:9202–7.
- 55 Saulle I, Vicentini C, Clerici M, Biasin M. An overview on ERAP roles in infectious diseases. *Cell*. 2020;**9**:720.
- 56 Pedersen MH, Hood BL, Beck HC, Conrads TP, Ditzel HJ, Leth-Larsen R. Downregulation of antigen presentation-associated pathway proteins is linked to poor outcome in triple-negative breast cancer patient tumors. *Oncotargets Ther*. 2017;**6**:e1305531.
- 57 Marin I, Boix O, Garcia-Garijo A, Sirois I, Caballe A, Zarzuela E, et al. Cellular senescence is immunogenic and promotes antitumor immunity. *Cancer Discov*. 2023;**13**:410–31.
- 58 Chen HA, Ho YJ, Mezzadra R, Adrover JM, Smolkin R, Zhu C, et al. Senescence rewires microenvironment sensing to facilitate antitumor immunity. *Cancer Discov*. 2023;**13**:432–53.
- 59 Dengel L, Burdick M, Stokes J, Strieter R, Mullins D, Bauer T, et al. Differential effects of IFN- α and IFN- γ on upregulation of IFN-inducible chemokines CXCL9, CXCL10 and CXCL11. *Cancer Res*. 2008;**68**:2149.
- 60 Frucht DM, Fukao T, Bogdan C, Schindler H, O'Shea JJ, Koyasu S. IFN-gamma production by antigen-presenting cells: mechanisms emerge. *Trends Immunol*. 2001;**22**:556–60.
- 61 Krummel MF, Mahale JN, Uhl LFK, Hardison EA, Mujal AM, Mazet JM, et al. Paracrine costimulation of IFN-gamma signaling by integrins modulates CD8 T cell differentiation. *Proc Natl Acad Sci U S A*. 2018;**115**:11585–90.
- 62 Chen Q, Coto-Llerena M, Suslov A, Teixeira RD, Fofana I, Nuciforo S, et al. Interferon lambda 4 impairs hepatitis C viral antigen presentation and attenuates T cell responses. *Nat Commun*. 2021;**12**:4882.
- 63 De Angelis C, Fu X, Cataldo ML, Nardone A, Pereira R, Veeraraghavan J, et al. Activation of the IFN signaling pathway is associated with resistance to CDK4/6 inhibitors and immune checkpoint activation in ER-positive breast cancer. *Clin Cancer Res*. 2021;**27**:4870–82.
- 64 Sun S, Frontini F, Qi W, Hariharan A, Ronner M, Wipplinger M, et al. Endogenous retrovirus expression activates type-I interferon signaling in an experimental mouse model of mesothelioma development. *Cancer Lett*. 2021;**507**:26–38.
- 65 Dai X, Cheng H, Bai Z, Li J. Breast cancer cell line classification and its relevance with breast tumor subtyping. *J Cancer*. 2017;**8**:3131–41.
- 66 Volcic M, Karl S, Baumann B, Salles D, Daniel P, Fulda S, et al. NF-kappaB regulates DNA double-strand break repair in conjunction with BRCA1-CtIP complexes. *Nucleic Acids Res*. 2012;**40**:181–95.
- 67 Zhao J, Zhang L, Lu A, Han Y, Colangelo D, Bukata C, et al. ATM is a key driver of NF-kappaB-dependent DNA-damage-induced senescence, stem cell dysfunction and aging. *Aging*. 2020;**12**:4688–710.
- 68 Wang B, Varela-Eirin M, Brandenburg SM, Hernandez-Segura A, van Vliet T, Jongbloed EM, et al. Pharmacological CDK4/6 inhibition reveals a p53-dependent senescent state with restricted toxicity. *EMBO J*. 2022;**41**:e108946.
- 69 Karl S, Pritschow Y, Volcic M, Hacker S, Baumann B, Wiesmuller L, et al. Identification of a novel pro-apoptotic function of NF-kappaB in the DNA damage response. *J Cell Mol Med*. 2009;**13**:4239–56.
- 70 Ruscetti M, Morris JP 4th, Mezzadra R, Russell J, Leibold J, Romesser PB, et al. Senescence-induced vascular remodeling creates therapeutic vulnerabilities in pancreas cancer. *Cell*. 2020;**181**:424–441.e21.
- 71 Xue W, Zender L, Miething C, Dickins RA, Hernando E, Krizhanovsky V, et al. Senescence and tumour clearance is triggered by p53 restoration in murine liver carcinomas. *Nature*. 2007;**445**:656–60.
- 72 Toso A, Revandkar A, Di Mitri D, Guccini I, Proietti M, Sarti M, et al. Enhancing chemotherapy efficacy in Pten-deficient prostate tumors by activating the senescence-associated antitumor immunity. *Cell Rep*. 2014;**9**:75–89.
- 73 Hong J, Jung M, Kim C, Kang M, Go S, Sohn H, et al. Senescent cancer cell-derived nanovesicle as a personalized therapeutic cancer vaccine. *Exp Mol Med*. 2023;**55**:541–54.

Supporting information

Additional supporting information may be found online in the Supporting Information section at the end of the article.

Fig. S1. Effects on cell viability and CDK4/6i-induced senescence with AI treatment. (A) MCF-7 cells were treated with AI (Anastrozole and Letrozole) in a dose-dependent manner for 5 days. Representative images are shown with a scale bar of 100 μm . Cell viability was measured after 5 days of AI treatment. (B) SA- β -gal staining was performed on MCF-7 cells treated with Palbociclib (2 μM) or a combination of Palbociclib and AI (Anastrozole and Letrozole; 2.5, 5, 10, 20, and 30 μM). Representative images are shown with a scale bar of 200 μm , and the percentage of stained cells was quantified and presented as a bar graph. The *P*-value was calculated using one-way ANOVA. ****P* < 0.001.

Fig. S2. Comparison of gene set enrichment analysis (GSEA) between control and TIS for immune

responses and angiogenesis. The comparison of enrichment score (ES), obtained from GSEA, between control and therapy-induced senescence (TIS) with gene sets related to (A) pro-tumorigenic immune response, (B) angiogenesis, and (C) anti-tumorigenic immune response; cutoff $P \leq 0.05$.

Fig. S3. Differential expression of pro-inflammatory SASP, pro-angiogenic factors, and anti-tumor immune-related genes between DNA-damaging agent- and CDK4/6i-induced senescence in HCC1428 breast cancer cells. (A) HCC1428 cells were treated with DNA-damaging agents (Cisplatin 5 μM and Doxorubicin 250 nM) and CDK4/6i (Palbociclib 5 μM) for 5 days and then SA- β gal staining was performed. Representative images of SA- β gal-positive cells are shown with a scale bar of 200 μm . The percentage of stained cells was quantified and presented as a bar graph. Data are mean \pm SD of three ($N = 3$) independent experiments. The P -value was calculated using one-way ANOVA. $***P < 0.001$. (B) mRNA expression level of cell cycle-related genes in senescent HCC1428 cells was measured by RT-qPCR. Data are mean \pm SD of three ($N = 3$) independent experiments. The P -value was calculated using one-way ANOVA. $*P < 0.05$ and $**P < 0.01$, and $***P < 0.001$. (C, D) The cells were harvested after 5 days of drug treatment and proteins were detected with immunoblotting. Data are representative of three ($N = 3$) independent experiments. (E–G) The cells were harvested after 5 days of drug treatment, and proteins and mRNA expression levels were measured by performing RT-qPCR. Data are mean \pm SD of three ($N = 3$) independent experiments. The P -value was calculated using one-way ANOVA. TIS vs. Control; $*P < 0.05$, $**P < 0.01$, $***P < 0.001$. Cis vs. Doxo and Palbo vs. Doxo; $\#P < 0.05$. (H) The cells (4×10^5 cells/100 mm dish) were treated and harvested after 5 days. The concentrations ($\text{pg}\cdot\text{mL}^{-1}$) of IL-6, CXCL8, VEGFA, CXCL10, and IFN- λ were measured by ELISA in conditioned media collected from senescent and control cells. Data are mean \pm SD of three ($N = 3$)

independent experiments. The P -value was calculated using one-way ANOVA. $*P < 0.05$ (TIS vs. Control) and $\#P < 0.05$ (Cis vs. Doxo, Palbo vs. Doxo). (I) The drug-treated HCC1428 cells were harvested after 5 days and p53, p21^{Waf1/Cip1} expression, and NF- κ B activation were determined by immunoblotting. β -actin was used as a loading control. Data are representative of three ($N = 3$) independent experiments.

Fig. S4. Differential expression of pro-inflammatory SASP, pro-angiogenic factors, and anti-tumor immune-related genes in senescence induced by DNA-damaging agents (Etoposide and Carboplatin) compared to CDK4/6i (Abemaciclib). (A) MCF-7 cells were treated with DNA-damaging agents (Etoposide 1 μM for 5 days and Carboplatin 75 μM for 5 days) and SA- β gal staining was performed. Representative images of SA- β gal-positive cells are shown with a scale bar of 200 μm . The percentage of stained cells was quantified and presented as a bar graph. Data are mean \pm SD of three independent experiments. The P -value was calculated using one-way ANOVA. $***P < 0.001$. (B) Protein expression was determined by immunoblotting. β -actin was used as a loading control. (C–E) MCF-7 cells were treated with DNA-damaging agents and CDK4/6i (Abemaciclib 1 μM for 5 days). The cells were harvested and subjected to RT-qPCR for mRNA expression levels. Data are mean \pm SD of three independent experiments. The P -value was calculated using one-way ANOVA. $*P < 0.05$, $**P < 0.01$, and $***P < 0.001$ (TIS vs. Control).

Fig. S5. Comparison of gene set enrichment analysis (GSEA) between control and TIS for p53, NF- κ B, and ESR1 signaling pathway. The comparison of enrichment score (ES), obtained from GSEA, between control and therapy-induced senescence (TIS) with gene sets related to (A) p53 signaling pathway, (B) NF- κ B signaling pathway, and (C) ESR1 signaling pathway; cutoff $P \leq 0.05$.

Table S1. List of Primer Sequences.